High-Performance Computational Models of Non-Hydrostatic Water Waves over Complex Bathymetry

Chris Kees[1,2], Eric Tovar[3,4], Rebecca Schurr[1], and Wen-Huai Tsao[1,2]
[1]Department of Civil and Environmental Engineering, Louisiana State University, Baton Rouge, LA; [2]Center for Computation and Technology, Louisiana State University, Baton Rouge, LA;
[3] U.S. Army Coastal and Hydraulics Laboratory, Vicksburg, MS; [4] Department of Mathematics, Texas A&M University, College Station, TX;

Introduction

Consider the propagation of periodic waves over a submerged bar as shown in Figure 1. In particular, we consider the experiments conducted by Beji and Battjes [1]. We show in Figure 1 the physical set-up of the experiments including the wave-maker, submerged trapezoidal bar (i.e., the bottom topography), wave absorption beach, and location of the wave gauges. In this scenario, we can observe the interaction of highly dispersive waves, particularly the release of higher-harmonics into a deeper region after the shoaling process. In this work, we consider three important numerical models of water wave propagation over variable bathymetry: the Serre-Green-Naghdi model of nonlinear dispersive shallow water waves, the fully nonlinear potential flow model, and the two-phase incompressible Navier-Stokes model. The immediate objective of the research is to understand the trade offs between physical fidelity and computational effort for this practical problem. The long term objective is to provide guidance for employing high-fidelity models for both local coastal engineering design and for informing sub-grid parameterizations in earth system models.

Figure 1 is a schematic diagram for the Beji experiments. All metrics in Figure 1 are in meters.

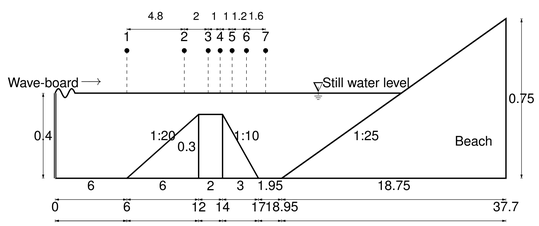

Figure 1: Definition sketch of wave flume and gauges.

Background

The model domain Ω can be separated into two subdomains: the water phase Ω_w and air phase Ω_a. The air-water interface (free surface), bottom bathymetry, wave inlet, wave outlet, and top boundary are denoted as Γ_f, Γ_b, Γ_i, Γ_o, and Γ, respectively. The two-phase model considers the entire model domain Ω and enforces mass and momentum conservation while modeling viscous effects and fully non-hydrostatic pressure effects. It requires a discretization of the entire domain Ω. The fully nonlinear potential flow model neglects the air phase as well as viscous effects in the water phase, by assuming the flow is irrotational, which allows the formulation of the problem as boundary integral equation on $\partial\Omega_w$. The Serre-Green-Naghdi model further neglects some (but not all) non-hydrostatic pressure effects, allowing the formulation of the problem as a hyperbolic partial differential equation on Γ_b [2]. Example cell and node distributions are shown in Figure 2.

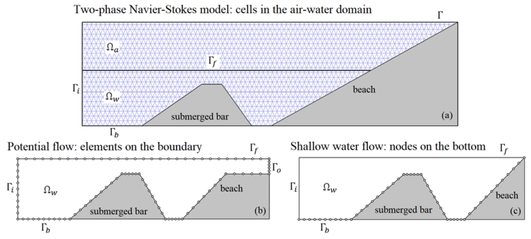

Figure 2: The computational domain and boundary with cell/element/node distribution of three numerical models.

Prior Work and Challenges

In prior work, we have developed a numerical laboratory combining level set methods and Finite Element Methods (FEMs) from Proteus (https://proteustoolkit.org) to develop two-phase Navier-Stokes numerical models as well as St. Venant and Serre-Green-Naghdi models [3, 2]. Our prior work includes model verification and validation as well as assessment of numerical errors and computational costs. In this study, we begin comparing these modeling approaches with the fully nonlinear potential flow model.

Two-Phase Navier-Stokes Model

The entire domain of this model consists of two incompressible Newtonian phases, air and water, separated by a sharp material interface, across which density and viscosity are discontinuous but velocity and pressure are continuous. Surface tension is neglected. The continuity and Navier-Stokes equations formulated for each phase of fluid are:

$$\nabla \cdot \mathbf{u_i} = 0 \tag{1}$$

$$\rho[\frac{\partial \mathbf{u_i}}{\partial t} + (\mathbf{u_i} \cdot \nabla)\mathbf{u_i}] = -\nabla\rho_i + \nabla \cdot \sigma_i + \mathbf{f} \tag{2}$$

where σ_i is the stress tensor, f is the body force, and w and a denotes the water and air phases, respectively. The proper boundary conditions on the air-water interface are provided based on the assumption of continuity of velocity and stress across the interface as:

$$p_a = p_w, \mathbf{u_a} = \mathbf{u_w}, \sigma_a \cdot \mathbf{n} = \sigma_w \cdot \mathbf{n} \text{on} \Gamma_f \tag{3}$$

By using this Eq.(8) and neglecting the potential loss of smoothness due to the jump discontinuities in density and viscosity, the continuous global pressure and velocity fields can be introduced so a single Navier-Stokes equations for the entire domain can be obtained as:

$$\nabla \cdot \mathbf{u} = 0 \tag{4}$$

$$\rho_w[\frac{\partial \mathbf{u}}{\partial t} + (\mathbf{u} \cdot \nabla)\mathbf{u}] = -\nabla\rho + \nabla \cdot (2\mu\epsilon) + \mathbf{f} \tag{5}$$

The two phases are separated by a sharp material interface, across which density and viscosity are discontinuous but velocity and pressure are continuous. Surface tension is neglected. Therefore the boundary conditions can be expressed as:

$$\rho = \rho_w H(\psi) + \rho_a[1 - H(\psi)] \tag{6}$$

$$\mu = \mu_w H(\psi) + \mu_a[1 - H(\psi)] \tag{7}$$

where H(ψ) is the Heaviside function expressed as:

$$H(\psi) = \begin{cases} 0 & , \psi < 0 \\ 1/2 & , \psi = 0 \\ 1 & , \psi > 0 \end{cases}$$

Potential Flow

This model assumes the fluid to be incompressible, inviscid, and irrotational. Therefore, the fluid velocity can be expressed by the gradient of the potential function ϕ. The continuity equation can be transferred into Laplace equation as:

$$\nabla^2\phi = 0 \tag{8}$$

By applying Green's second identity to Eq. (8), the boundary integral equation (BIE) can be obtained as:

$$c_p\phi_p = \int_{\partial\Omega_w} (\frac{\partial G}{\partial n}\phi - G\frac{\partial \phi}{\partial n})d\Gamma \tag{9}$$

where G is the fundamental solution with source point p and c_p is the resulting flux. As the source point x_p is placed on the boundary of water domain, the BIE becomes a truly 'boundary-only' equation so numerical methods such as the Boundary Element Method (BEM) can be employed on the boundary to rewrite Eq. (9) in matrix form as:

$$\mathbf{A}\phi = \mathbf{B}\frac{\partial \phi}{\partial n} \tag{10}$$

The mixed type boundary value problem arises with Dirichlet condition applied to the free surface and Neumann condition applied to the wetted boundaries. Therefore the free surface is updated through the second-order Taylor series expansion during a small time step Δt as:

$$\xi(t + \Delta t) = \xi(t) + \Delta t\frac{D\xi}{Dt} + \frac{\Delta t^2}{2}\frac{D^2\xi}{Dt^2} + O[\Delta t^3] \tag{11}$$

$$\phi(t + \Delta t) = \phi(t) + \Delta t\frac{D\phi}{Dt} + \frac{\Delta t^2}{2}\frac{D^2\phi}{Dt^2} + O[\Delta t^3] \tag{12}$$

A new variable $\phi_t = \frac{\partial \phi}{\partial t}$ appears in the second-order term in Eqs. (11) and (12). Since ϕ_t also satisfies the Laplace's equation, another BIE for ϕ_t and ϕ_{t_n} needs to be solved. Fortunately, the domain geometry remains unchanged at the current time step so **A** and **B** as shown in Eq. (10) can be reused. Therefore the free-surface tracking is very fast. A complete description of the numerical solution is presented in [4]. Since the nodal computational degrees of freedom are located only on the boundary $\partial\Omega_w$, the computational cost can be significantly smaller than for the two-phase approach.

Dispersive Shallow Water Flow

We consider the Serre–Green–Naghdi (SGN) Equations for modeling dispersive shallow water waves. The SGN equations form a nonlinear system of partial differential equations and are considered to be a more realistic model compared to the classical Saint-Venant model. In particular, the SGN model is an $\mathcal{O}(\mu^2)$ approximation of the free surface Euler Equations. Even though it's a depth-averaged model, it accounts for effects due to vertical acceleration of the fluid. Letting h denote the water depth, $\boldsymbol{v}$ the depth-averaged velocity and z the topography map, the equations can be written as follows:

$$\partial_t \mathrm{h} + \nabla\cdot(\mathrm{h}\boldsymbol{v}) = 0, \tag{13}$$

$$\partial_t(\mathrm{h}\boldsymbol{v}) + \nabla\cdot(\boldsymbol{v}\otimes\mathrm{h}\boldsymbol{v}) + \nabla p = -\big(g\mathrm{h} + \mathrm{D}_t^2(\frac{1}{2}\mathrm{h} + z)\big)\nabla z, \tag{14}$$

$$p = \frac{1}{2}g\mathrm{h}^2 + \frac{1}{3}\mathrm{h}^2\mathrm{D}_t^2(\mathrm{h} + \frac{3}{2}z). \tag{15}$$

We consider the method presented in [2], which results in a discretization of field quantities only along Γ_b.

Results

In the experiment, the sinusoidal long waves have amplitude A = 1 cm and period T = 2s. Since the wave speed changes over the bottom topography, the dispersive characteristics can be observed through the wave elevations recorded by the wave gauges installed ahead and behind the bar as shown in Fig. 3. During the wave propagation, as higher harmonics are released, the nonlinearity becomes significant, and waves steepen during the shoaling process. The three numerical results are in good agreement with the measurements. The two-phase flow model has more reduction in wave magnitude. Slight phase shifts were observed at wave gauges 6 and 7 but the wave frequencies were well predicted.

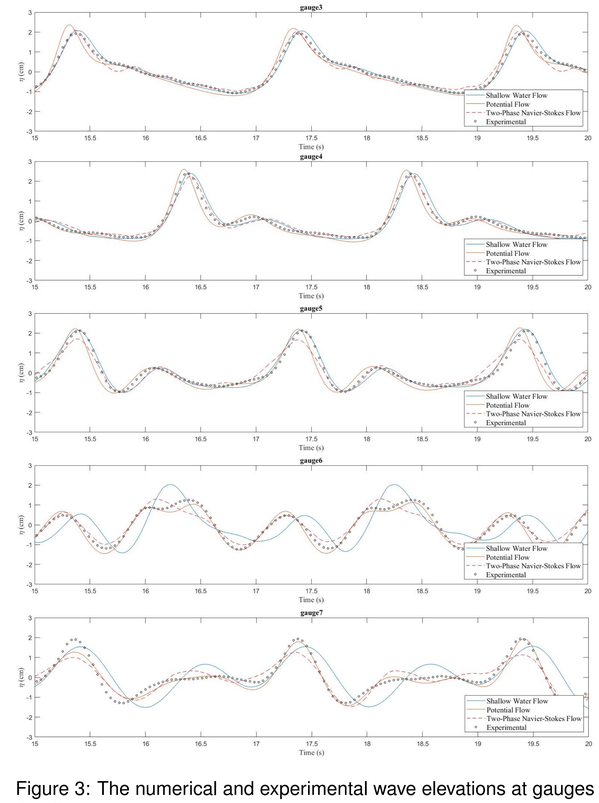

Figure 3: The numerical and experimental wave elevations at gauges 3 to 7.

Future Work

While the results show overall agreement, additional refinement in space and time will be considered to demonstrate grid independent convergence, which will allow assessment of the relevance of viscous and non-hydrostatic physical effects. More detailed comparisons of wall clock time and computational effort will also be conducted to assess the varying computational trade offs. The bathymetry considered is relatively smooth, while in reality discontinuous bathymetry is common and triggers different hydrodynamic processes. Future work will consider a more complete set of benchmarks to clarify modeling trade offs over a wider set of realistic conditions.

References

[1] S. Beji and J. A. Battjes. Numerical simulation of nonlinear wave propagation over a bar. *Coastal Engineering*, 23(1):1–16, May 1994.

[2] Jean-Luc Guermond, Chris Kees, Bojan Popov, and Eric Tovar. Hyperbolic relaxation technique for solving the dispersive Serre–Green–Naghdi equations with topography. *Journal of Computational Physics*, page 110809, November 2021.

[3] C. E. Kees, I. Akkerman, M. W. Farthing, and Y. Bazilevs. A conservative level set method suitable for variable-order approximations and unstructured meshes. *Journal of Computational Physics*, 230(12):4536–4558, June 2011.

[4] S. T. Grilli, J. Skourup, and I. A. Svendsen. An efficient boundary element method for nonlinear water waves. *Engineering Analysis with Boundary Elements*, 6(2):97–107, June 1989.